

Energy-Calibrated VAE with Test Time Free Lunch

Yihong Luo^{1,2}, Siya Qiu^{1,2}, Xingjian Tao¹, Yujun Cai³, and Jing Tang^{1,2}

¹ The Hong Kong University of Science and Technology (Guangzhou)

² The Hong Kong University of Science and Technology ³ Meta
 yluocg@connect.ust.hk, jingtang@ust.hk

Abstract. In this paper, we propose a novel generative model that utilizes a conditional Energy-Based Model (EBM) for enhancing Variational Autoencoder (VAE), termed Energy-Calibrated VAE (EC-VAE). Specifically, VAEs often suffer from blurry generated samples due to the lack of a tailored training on the samples generated in the generative direction. On the other hand, EBMs can generate high-quality samples but require expensive Markov Chain Monte Carlo (MCMC) sampling. To address these issues, we introduce a conditional EBM for calibrating the generative direction of VAE during training, without requiring it for the generation at test time. In particular, we train EC-VAE upon both the input data and the calibrated samples with adaptive weight to enhance efficacy while avoiding MCMC sampling at test time. Furthermore, we extend the calibration idea of EC-VAE to variational learning and normalizing flows, and apply EC-VAE to an additional application of zero-shot image restoration via neural transport prior and range-null theory. We evaluate the proposed method with two applications, including image generation and zero-shot image restoration, and the experimental results show that our method achieves competitive performance over single-step non-adversarial generation.

Keywords: Image Generation · VAEs · EBMs

1 Introduction

Deep generative models, including Generative Adversarial Nets (GANs) [14], Variational Autoencoders (VAEs) [28], flow-based generative models [8,9], Energy-Based Models (EBMs) [10,56], and diffusion models [23], achieve excellent performance in a variety of applications. Compared to GANs, likelihood-based models, such as VAEs and EBMs, typically exhibit greater stability during training and more faithfully cover modes in the data. Moreover, unlike normalizing flows that suffer from architecture restrictions [30], VAEs and EBMs offer considerable potential for expressivity. Therefore, VAEs and EBMs have gained extensive attention recently.

In particular, VAEs map the input data into a latent distribution and optimize the evidence lower bound (ELBO) on the data likelihood. However, VAEs

do not explicitly optimize the generative direction. Specifically, VAEs assume that the prior distribution in latent space (e.g., Gaussian distribution) matches the empirical distribution mapped from the input data. Unfortunately, there is often a gap between the two distributions in practice. As a result, VAEs struggle to generate high-quality images, producing blurry or corrupted samples. To tackle this issue, in addition to designing more flexible prior distribution [1, 48, 59], some work [21, 43, 49] involves GANs, yielding unstable adversarial games, while NVAE [50] proposes to adjust BatchNorm [22] statistics based on prior distribution that improves the generation slightly.

On the other hand, EBMs directly model the unnormalized density in data space by assigning low energy to high-probability areas. Unlike VAEs that usually assume a Gaussian prior, EBMs do not necessitate distribution assumptions in modeling. In fact, EBMs have shown comparable state-of-the-art performance in terms of generative results among non-adversarial methods [32]. However, a significant drawback of EBMs is the necessity for Markov Chain Monte Carlo (MCMC) sampling during the training and during the generation at test time, which suffers from slow convergence and is computationally expensive, particularly when the energy is parameterized by neural networks.

In this paper, we propose a novel generative model termed Energy-Calibrated VAE (EC-VAE) by involving a conditional EBM to calibrate the VAE for better generation while keeping high sampling efficiency. The VAE is trained by ELBO and the energy-based calibration. Specifically, to address the training of the generative side that is missing in the conventional VAE, we propose to incorporate the generated samples into training. That is, for the generated data $\hat{\mathbf{x}}$ by the generative model, we use a conditional EBM to sample data $\tilde{\mathbf{x}}$ initialized with $\hat{\mathbf{x}}$ that approximates the input real data. Then, integrating the minimization of the distance between $\hat{\mathbf{x}}$ and $\tilde{\mathbf{x}}$ into training can calibrate the decoder. We show that the proposed model can be jointly trained by adopting the primal-dual method in a constrained formulation. The conditional EBM is solely utilized for calibrating samples. Consequently, a short-run MCMC sampling is sufficient and does not suffer from slow convergence. Note that the EBM is involved in training (i.e., generation calibration) only, and is not required during test time sampling.

Moreover, we show that the idea of energy-based calibration can be extended to calibrate the variational inference and normalizing flows with large improvement. Take the former as an illustration while the latter is similar. We first sample \mathbf{z} from variational posterior, and then calibrate \mathbf{z} by running MCMC sampling on constructed conditional posterior $p(\tilde{\mathbf{z}}|\mathbf{z}, \mathbf{x})$ to obtain the calibrated $\tilde{\mathbf{z}}$. Finally, minimizing the distance between \mathbf{z} and $\tilde{\mathbf{z}}$ can calibrate the encoder.

Experimental results show that the proposed EC-VAE outperforms previous EBMs and the state-of-the-art VAEs on image generation benchmarks in both low-resolution and high-resolution datasets by a large margin. In particular, EC-VAE achieves the strong performance with a single-step non-adversarial generation manner, competing with advanced GANs and diffusions across multiple datasets. We also propose and show how to apply EC-VAE to image restora-

tion in a zero-shot way by constructing neural transport prior and leveraging range-null space theory with competitive performance.

Our main contributions are summarized as follows.

1. We propose a new generative model termed EC-VAE utilizing a conditional EBM to calibrate the VAE to generate sharper samples without incurring extra costs of MCMC sampling during the generation at test time.
2. We extend the energy-based calibration to enhance variational learning and normalizing flows, and apply EC-VAE to an additional application of zero-shot image restoration.
3. We demonstrate the strong empirical results of our proposed methods on various tasks, including image generation and image restoration.

2 Preliminaries

2.1 Notations

Denote by \mathbf{x} the data and by \mathbf{z} the latent variable. Let \mathcal{X} be the data space and \mathcal{Z} be the latent space. Let $p_d(\mathbf{x})$ be the data distribution. Denote by $f_\alpha: \mathcal{X} \rightarrow \mathcal{Z}$ the encoder parameterized by α , and by $g_\beta: \mathcal{Z} \rightarrow \mathcal{X}$ the decoder parameterized by β . Denote by $E_\omega: \mathcal{X} \rightarrow \mathbb{R}$ the energy function parameterized by ω .

2.2 Variational Autoencoders

VAE [29] adopts the encoder-decoder architecture with a prior distribution. To be more precise, VAE defines the joint distribution of (\mathbf{x}, \mathbf{z}) as $p_{\beta, \theta}(\mathbf{x}, \mathbf{z}) = p_\beta(\mathbf{x}|\mathbf{z})p_\theta(\mathbf{z})$. The model can be trained by maximizing the marginal log-likelihood $\mathcal{L} = \mathbb{E}_{p_d(\mathbf{x})}[\log p_{\beta, \theta}(\mathbf{x})]$. However, maximizing the log-likelihood needs sampling from intractable posterior $p_{\beta, \theta}(\mathbf{z}|\mathbf{x}) = \frac{p_{\beta, \theta}(\mathbf{x}, \mathbf{z})}{p_\beta(\mathbf{x})}$.

Instead of sampling from intractable posterior $p_{\beta, \theta}(\mathbf{z}|\mathbf{x})$, VAEs propose using a variational inference $q_\alpha(\mathbf{z}|\mathbf{x})$ to approximate the posterior. In particular, VAEs optimize the evidence lower bound (ELBO) on $\log p_{\beta, \theta}(\mathbf{x})$ such that

$$\text{ELBO}_\phi(\mathbf{x}) = \mathbb{E}_{q_\alpha(\mathbf{z}|\mathbf{x})}[\log p_\beta(\mathbf{x}|\mathbf{z}) - \text{KL}(q_\alpha(\mathbf{z}|\mathbf{x})||p_\theta(\mathbf{z}))], \quad (1)$$

where $\phi = \{\alpha, \beta, \theta\}$. The first term is the reconstruction loss and the second term is the KL divergence between the approximated posterior and the prior.

Sampling from VAE. The sampling procedure of VAE is to sample \mathbf{z} from prior $p_\theta(\mathbf{z})$ first, and then obtain generated samples \mathbf{x} with probability $p_\beta(\mathbf{x}|\mathbf{z}) = \mathcal{N}(g_\beta(\mathbf{z}), \sigma^2 \mathbf{I})$. Equivalently, we denote samples $\mathbf{x} \sim p_{\beta, \theta}(\mathbf{x}) = \int p_\theta(\mathbf{z})p_\beta(\mathbf{x}|\mathbf{z})d\mathbf{z}$. In practice, the samples are typically obtained directly by $g_\beta(\mathbf{z})$.

2.3 Energy-Based Models

A deep EBM assumes that $p_\omega(\mathbf{x})$ is a gibbs distribution with the form $p_\omega(\mathbf{x}) = \exp(-E_\omega(\mathbf{x}))/L_\omega$, where L_ω is the corresponding normalizing constant. EBM is

trained by minimizing the negative log-likelihood (NLL) $\mathcal{L}(\omega)$ such that

$$\mathcal{L}(\omega) = -\mathbb{E}_{p_d(\mathbf{x})}[\log p_\omega(\mathbf{x})] = -\mathbb{E}_{p_d(\mathbf{x})}\left[\frac{\exp(-E_\omega(\mathbf{x}))}{L_\omega}\right].$$

The gradient of $\mathcal{L}(\omega)$ can be obtained as follows:

$$\nabla \mathcal{L}(\omega) = \mathbb{E}_{p_d(\mathbf{x})}[\nabla E_\omega(\mathbf{x})] - \mathbb{E}_{p_\omega(\mathbf{x})}[\nabla E_\omega(\mathbf{x})]. \quad (2)$$

In practice, sampling from $p_\omega(\mathbf{x})$ can be achieved by running MCMC sampling with K steps of Langevin dynamics, with given initial samples \mathbf{x}_0 and step size s :

$$\mathbf{x}_{k+1} = \mathbf{x}_k - \frac{s}{2} \nabla_{\mathbf{x}_k} E_\omega(\mathbf{x}_k) + \sqrt{s} \xi, \quad \text{where } \xi \sim \mathcal{N}(0, \mathbf{I}).$$

2.4 Additional Related Work

Our method shares some similarities with works that combine generative autoencoders and EBMs in different ways. VAEBM [53] learns EBM upon a pre-trained NVAE [50], and a recent work [15] jointly learns EBM and VAE by an adversarial game instead of by MCMC sampling, while our work is jointly trained without adversarial components. In addition, our learning algorithm bears some similarities to cooperative learning [19, 55, 57, 58], which also employs EBM to teach the base generative model, but only in small images. However, the base generative model in these approaches is purely trained upon *generated samples*, which can be quite biased. In contrast, our base generative model (i.e., VAE) is trained upon data and generated samples, with adaptive weights. Recently, dual MCMC [6] also consider incorporating real data into cooperative-like training. However, similar to other cooperative approaches [55, 57], they maximize the *marginal likelihood* of the generated samples by latent variable models. This requires extra effort in inferring latent variables, increasing the burden of the model and training cost. In contrast, we maximize the *conditional likelihood* of the generated samples via the decoder of VAE, which is easier to learn. Moreover, our method differs significantly from aforementioned works in the way that we discard MCMC during inference without adversarial components, providing a strong one-step generation that competes with diffusions and GANs.

3 The Design of Energy-Calibrated VAE

An issue with VAE is that the generative direction has not been explicitly trained during the training process, potentially leading to lower-quality output for the generated samples. To address this, we propose to incorporate the generated samples into the training. As the real data corresponding to the generated samples are unavailable, we propose utilizing a short-run MCMC, initialized with the generated samples, to approximate the corresponding real data.

As the aim is to calibrate the samples, we suggest constructing a **conditional EBM**, similar in [12], to model the conditional density, i.e.,

$$p_\omega(\tilde{\mathbf{x}}|\mathbf{x}) = \frac{1}{L_\omega(\mathbf{x})} \exp(-E_\omega(\tilde{\mathbf{x}}) - \frac{\|\tilde{\mathbf{x}} - \mathbf{x}\|_2^2}{2\sigma^2}),$$

where σ is a pre-defined hyper-parameter, $L_\omega(\mathbf{x}) = \int \exp(-E_\omega(\tilde{\mathbf{x}}) - \frac{\|\tilde{\mathbf{x}} - \mathbf{x}\|_2^2}{2\sigma^2}) d\tilde{\mathbf{x}}$ is the corresponding normalizing constant, \mathbf{x} is the generated samples from VAE, E_ω is an unconditional EBM. Compared to direct model $p_\omega(\tilde{\mathbf{x}})$, the extra distance term in $p_\omega(\tilde{\mathbf{x}}|\mathbf{x})$ constrains the high-density area localized around generated samples \mathbf{x} , making it easier to be learned by the base generative model (i.e., VAE). Sampling from $p_\omega(\tilde{\mathbf{x}}|\mathbf{x})$ can be achieved by MCMC with Langevin dynamics, i.e.,

$$\mathbf{x}_{k+1} = \mathbf{x}_k - \frac{s}{2} \left(\underbrace{\nabla_{\mathbf{x}_k} E_\omega(\mathbf{x}_k)}_{\text{direct to real}} + \underbrace{\nabla_{\mathbf{x}_k} \frac{\|\mathbf{x}_k - \mathbf{x}\|_2^2}{2\sigma^2}}_{\text{direct to origin}} \right) + \sqrt{s}\xi, \quad \text{where } \xi \sim \mathcal{N}(0, \mathbf{I}). \quad (3)$$

For simplicity, we denote $\mathbf{x}^K = \text{MCMC}_\omega^K(\tilde{\mathbf{x}}|\mathbf{x})$. The learning of EBM can be achieved by minimizing $\mathcal{L}(\omega) \triangleq \mathbb{E}_{p_{\beta,\theta}(\mathbf{x})}[D_{\text{KL}}(p_d(\tilde{\mathbf{x}}|\mathbf{x})||p_\omega(\tilde{\mathbf{x}}|\mathbf{x}))]$:

$$\begin{aligned} \nabla \mathcal{L}(\omega) &= \mathbb{E}_{p_{\beta,\theta}(\mathbf{x})} [\mathbb{E}_{p_d(\tilde{\mathbf{x}}|\mathbf{x})} [\nabla_\omega \log p_\omega(\tilde{\mathbf{x}}|\mathbf{x})] - \mathbb{E}_{p_\omega(\tilde{\mathbf{x}}|\mathbf{x})} [\nabla_\omega \log p_\omega(\tilde{\mathbf{x}}|\mathbf{x})]] \\ &= \mathbb{E}_{p_{\beta,\theta}(\mathbf{x})} [\mathbb{E}_{p_d(\tilde{\mathbf{x}}|\mathbf{x})} [\nabla_\omega E_\omega(\tilde{\mathbf{x}})]] - \mathbb{E}_{p_{\beta,\theta}(\mathbf{x})} [\mathbb{E}_{p_\omega(\tilde{\mathbf{x}}|\mathbf{x})} [\nabla_\omega E_\omega(\tilde{\mathbf{x}})]] \\ &= \mathbb{E}_{p_d(\tilde{\mathbf{x}})} [\nabla_\omega E_\omega(\tilde{\mathbf{x}})] - \mathbb{E}_{p_{\beta,\theta}(\mathbf{x})} [\mathbb{E}_{p_\omega(\tilde{\mathbf{x}}|\mathbf{x})} [\nabla_\omega E_\omega(\tilde{\mathbf{x}})]]. \end{aligned}$$

Since the distance term does not involve learnable parameters, hence the parameter ω can be learned in unconditional form. We only need to define $p_d(\tilde{\mathbf{x}}|\mathbf{x})$ to ensure the marginal distribution of $p_{\beta,\theta}(\mathbf{x})p_d(\tilde{\mathbf{x}}|\mathbf{x})$ being data distribution (e.g., the simplest case is $p_d(\tilde{\mathbf{x}}|\mathbf{x}) \triangleq p_d(\tilde{\mathbf{x}})$). It can be seen that the $\mathcal{L}(\omega)$ reaches minima at $\int p_{\beta,\theta}(\mathbf{x})p_\omega(\tilde{\mathbf{x}}|\mathbf{x})d\mathbf{x} = p_d(\tilde{\mathbf{x}})$. This is said that given rich enough $p_\omega(\tilde{\mathbf{x}}|\mathbf{x})$, we are able to calibrate samples from $p_{\beta,\theta}(\mathbf{x})$ to $p_d(\tilde{\mathbf{x}})$.

Then, we regard the $\tilde{\mathbf{x}}$ as calibrated samples, thus the generative direction can be calibrated by minimizing the distance between \mathbf{x} and $\tilde{\mathbf{x}}$,

$$\mathcal{L}_{\text{calibration}} = \mathbb{E}_{p_{\beta,\theta}(\mathbf{x})} [\mathbb{E}_{p_\omega(\tilde{\mathbf{x}}|\mathbf{x})} [\|\mathbf{x} - \tilde{\mathbf{x}}\|_2^2]].$$

Note that the calibration loss can be considered as maximizing the likelihood of calibrated samples conditioned on generated samples under the form of normal distribution. This MCMC for sampling calibrated $\tilde{\mathbf{x}}$ can be regarded as a teacher, guiding the generative model to produce higher-quality generated samples. However MCMC sampling introduces some random noise into training, making it impossible to perfectly match the calibrated samples, thus we suggest using a constrained optimization form as follows:

Definition 1 (Energy-Calibrated VAE) *Given a fixed margin ϵ_1 , the general optimization can be transformed into the following inequality-constrained optimization.*

$$\begin{aligned} \min_{\phi, \omega} \quad & \mathcal{L}(\phi) + \mathcal{L}(\omega) \\ \text{s.t.} \quad & \|\tilde{\mathbf{x}} - \mathbf{x}\|_2^2 < \epsilon_1, \quad \forall \mathbf{x} \sim p_{\beta,\theta}(\mathbf{x}), \tilde{\mathbf{x}} = \text{MCMC}_\omega^K(\tilde{\mathbf{x}}|\mathbf{x}), \\ \text{where} \quad & \mathcal{L}(\omega) = \mathbb{E}_{p_{\beta,\theta}(\mathbf{x})} D_{\text{KL}}(p_d(\tilde{\mathbf{x}}|\mathbf{x})||p_\omega(\tilde{\mathbf{x}}|\mathbf{x})), \\ & \mathcal{L}(\phi) = -\mathbb{E}_{p_d(\mathbf{z})} \mathbb{E}_{q_\alpha(\mathbf{z}|\mathbf{x})} [\log p_\beta(\mathbf{x}|\mathbf{z}) - \frac{q_\alpha(\mathbf{z}|\mathbf{x})}{p_\theta(\mathbf{z})}]. \end{aligned}$$

We get a constrained optimization problem in Definition 1, which is hard to optimize directly, but we can consider it as a corresponding saddle-point problem as follows:

$$\max_{\lambda} \min_{\phi, \omega} \{ \mathcal{L}(\phi) + \mathcal{L}(\omega) + \lambda \mathcal{L}_{\text{con}}(\phi) \}, \quad \lambda \geq 0$$

where the constraint-related loss $\mathcal{L}_{\text{con}}(\phi)$ is defined as:

$$\mathcal{L}_{\text{con}}(\phi) = \mathcal{L}_{\text{con}}(\beta) = \mathbb{E}_{p_{\beta, \theta}(\mathbf{x})} [\mathbb{E}_{p_{\omega}(\tilde{\mathbf{x}}|\mathbf{x})} [\|\mathbf{x} - \tilde{\mathbf{x}}\|_2^2 - \epsilon_1]].$$

Since the prior is typically less powerful, we suggest calibrating only the decoder, enabling the prior focus on maximizing likelihood related to the latent variable.

The final challenge is the lack of access to the ground truth of data distribution. To tackle this issue, we consider the corresponding empirical optimization problem as follows:

$$\begin{aligned} & \max_{\lambda} \min_{\phi, \omega} \{ \hat{\mathcal{L}}(\phi) + \hat{\mathcal{L}}(\omega) + \lambda \mathcal{L}_{\text{con}}(\phi) \} \\ & = \max_{\lambda} \min_{\phi, \omega} \left\{ \sum_{i=1}^n \sum_{j=1}^m - \left(\log p_{\beta}(\mathbf{x}_i | \mathbf{z}_{ij}) + \log \frac{q_{\alpha}(\mathbf{z}_{ij} | \mathbf{x}_i)}{p_{\theta}(\mathbf{z}_{ij})} \right) + \sum_{i=1}^n - \log p_{\omega}(\mathbf{x}_i) \right. \\ & \quad \left. + \lambda \sum_{i=1}^n [\|\hat{\mathbf{x}}_i - \text{MCMC}_{\omega}^K(\tilde{\mathbf{x}}_i | \hat{\mathbf{x}}_i)\|_2^2 - \epsilon_1] \right\}, \end{aligned}$$

where \mathbf{x}_i is sampled from data, $\hat{\mathbf{x}}_i$ is sampled from the VAE, \mathbf{z}_{ij} is sampled from $q_{\alpha}(\mathbf{z} | \mathbf{x}_i)$. Notice that m is usually chosen to be one in practice that is efficient and effective enough to estimate the gradient. MCMC is not necessary during test time sampling.

Concrete Algorithm. To efficiently optimize the problem, we employ the primal-dual algorithm tailored for addressing the saddle-point problem corresponding to the constrained form. Specifically, in the *primal* step, the algorithm alternately optimizing parameters ω and $\phi = \{\beta, \alpha, \theta\}$ by minimizing the empirical Lagrangian under a given dual variable λ , i.e.,

$$\begin{aligned} \omega_{t+1} &:= \arg \min_{\omega} \hat{\mathcal{L}}(\omega_t), \\ \beta_{t+1} &:= \arg \min_{\beta} \left\{ \lambda \hat{\mathcal{L}}_{\text{con}}(\beta_t) - \sum_{i=1}^n \sum_{j=1}^m \log p_{\beta_t}(\mathbf{x}_i | \mathbf{z}_{ij}) \right\}, \\ \alpha_{t+1} &:= \arg \min_{\alpha} \left\{ \sum_{i=1}^n \sum_{j=1}^m \log \frac{q_{\alpha_t}(\mathbf{z}_{ij} | \mathbf{x}_i)}{p_{\theta_t}(\mathbf{z}_{ij})} - \log p_{\beta_t}(\mathbf{x}_i | \mathbf{z}_{ij}) \right\}, \\ \theta_{t+1} &:= \arg \min_{\theta} \left\{ \sum_{i=1}^n \sum_{j=1}^m - \log p_{\theta_t}(\mathbf{z}_{ij}) \right\}. \end{aligned}$$

In practice, we perform stochastic gradient descent that derives concrete update step for θ and ϕ . On the other hand, in the *dual* step, we update λ as follows,

$$\lambda_{t+1} := \max \left\{ \lambda_t + \eta \cdot (\hat{\mathcal{L}}_{\text{con}} - \epsilon), 0 \right\}, \quad (4)$$

where η is the learning rate of dual step.

Algorithm 1 in Appendix A gives the pseudo-code of our primal-dual algorithm for optimizing the VAE parameters ϕ , and EBMs parameters ω . Compared

with using stochastic gradient descent directly in the constrained optimization problem in Definition (1), the primal-dual algorithm can dynamically tune λ to avoid introducing extra hyper-parameters (which may serve as an early-stopping condition, e.g., $\lambda = 0$), and can provide convergence guarantees with sufficiently long training using sufficiently small step size [3].

4 Extensions and Additional Application

In this section, we first show the calibration idea of EC-VAE can be extended to enhance variational learning and normalizing flows. Then we show how to apply our method in zero-shot image restoration.

4.1 Energy-Calibrated Variational Learning

Variational learning allows efficient training, but results in learning a lower bound for data likelihood. The gap is the KL divergence between variational posterior $q_\alpha(\mathbf{z}|\mathbf{x})$ and posterior $p_{\beta,\theta}(\mathbf{z}|\mathbf{x})$ which is not explicitly minimized in variational training, just like the training of the generative direction is missing in vanilla VAEs.

Similar to calibrating the generative direction as proposed in Sec. 3, we propose to incorporate the calibration of the variational posterior $q_\alpha(\mathbf{z}|\mathbf{x})$ into training. We first construct the conditional density $p_{\beta,\theta}(\tilde{\mathbf{z}}|\mathbf{z}, \mathbf{x})$ as follows:

$$p_{\beta,\theta}(\tilde{\mathbf{z}}|\mathbf{z}, \mathbf{x}) = p_{\beta,\theta}(\tilde{\mathbf{z}}|\mathbf{x}) \cdot \exp\left(-\frac{\|\tilde{\mathbf{z}}-\mathbf{z}\|_2^2}{2\sigma^2}\right)/L_{\beta,\theta}(\mathbf{z}),$$

where σ is a pre-defined hyper-parameter, $p_{\beta,\theta}(\tilde{\mathbf{z}}|\mathbf{x})$ is the posterior and $L_{\beta,\theta}(\mathbf{z})$ is corresponding normalizing constant. The conditional density is constructed by adding the distance term to constrain the calibrated \mathbf{z} to be close to \mathbf{z} . And the sampling can be achieved by MCMC with Langevin dynamics. Given a step size $s > 0$ and an initial value \mathbf{z}_0 , the Langevin dynamics iterates:

$$\mathbf{z}_{k+1} = \mathbf{z}_k - \frac{s}{2} \nabla_{\mathbf{z}_k} (-\log p_{\beta,\theta}(\mathbf{z}_k|\mathbf{x}) + \frac{\|\mathbf{z}_k - \mathbf{z}\|_2^2}{2\sigma^2}) + \sqrt{s}\xi, \quad \xi \sim \mathcal{N}(0, \mathbf{I})$$

where the \mathbf{z}_0 is proposed to be sampled from variational posterior $q_\alpha(\mathbf{z}|\mathbf{x})$, thus the \mathbf{z}_K can be considered as calibrated \mathbf{z} . For simplicity, we denote $\mathbf{z}^K = \text{MCMC}_{\beta,\theta}^K(\tilde{\mathbf{z}}|\mathbf{z})$. Note the $\nabla_{\mathbf{z}} \log p_{\beta,\theta}(\mathbf{z}|\mathbf{x})$ can be easily obtained by following form: $\nabla_{\mathbf{z}} \log p_{\beta,\theta}(\mathbf{z}|\mathbf{x}) = \nabla_{\mathbf{z}} \log p_{\beta,\theta}(\mathbf{x}, \mathbf{z}) - \nabla_{\mathbf{z}} \log p_{\beta,\theta}(\mathbf{x}) = \nabla_{\mathbf{z}} \log p_{\beta,\theta}(\mathbf{x}, \mathbf{z})$.

Once the MCMC Calibrated \mathbf{z}_K is obtained, we can conduct the constrained learning formulation similar to Sec. 3. We directly give the corresponding saddle-point problem:

$$\mathcal{L}(\phi = \{\alpha, \beta, \theta\}) = -\mathbb{E}_{p_d(\mathbf{x})}[\text{ELBO}_\phi(\mathbf{x})] + \lambda_1 \cdot \mathcal{L}_{\text{con}}(\beta) + \lambda_2 \cdot \mathcal{L}_{\text{con}}(\alpha), \quad \lambda_1, \lambda_2 \geq 0,$$

where $\mathcal{L}_{\text{con}}(\alpha) = \mathbb{E}_{q_\alpha(\mathbf{z}|\mathbf{x})}[\mathbb{E}_{p_{\beta,\theta}(\tilde{\mathbf{z}}|\mathbf{z}, \mathbf{x})}[\|\mathbf{z} - \tilde{\mathbf{z}}\|_2^2]]$. Given the saddle-point formulation, the learning and calibration of the encoder parameterized by α can be

achieved with corresponding empirical optimization as follows:

$$\alpha_{t+1} := \arg \min_{\alpha} \left\{ \sum_{i=1}^n \sum_{j=1}^m \left(\log \frac{q_{\alpha_t}(\mathbf{z}_{ij}|\mathbf{x}_i)}{p_{\theta_t}(\mathbf{z}_{ij})} - \log p_{\beta_t}(\mathbf{x}_i|\mathbf{z}_{ij}) \right) + \lambda_2 \times \|\mathbf{z}_{ij} - \text{MCMC}_{\beta,\theta}^K(\tilde{\mathbf{z}}_{ij}|\mathbf{z}_{ij})\|_2^2 \right\},$$

The update of the rest parameters $\{\beta, \theta, \omega\}$ remain the same, while the λ_i ($i=1,2$) is updated by Eq. (4).

4.2 Energy-Calibrated Normalizing Flow

The Energy-Calibrated Normalizing Flow (EC-Flow) can be easily formed, as normalizing flow h_{ϕ} directly models the data likelihood $p_{\phi}(\mathbf{x}) = p_z(\mathbf{z}) \times \left| \det \left(\frac{\partial h_{\phi}}{\partial \mathbf{z}} \right) \right|$, where h_{ϕ} is the invertible transformation, thus we just need to use the negative log-likelihood $-\mathbb{E}_{p_d(\mathbf{x})}[\log p_{\phi}(\mathbf{x})]$ estimated by normalizing flow to serve as the $\mathcal{L}(\phi)$, and directly sampling from $p_{\phi}(\mathbf{x})$ to obtain samples, while other components keep the same.

4.3 Applying to Zero-Shot Image Restoration

In this section, we present the application of our method in zero-shot image restoration tasks, inspired by recent works [52] that employ the diffusion model and the Range-Null space theory for similar purposes.

We start by briefly reviewing the necessary background. Given a known linear operator $\mathbf{A} \in \mathbb{R}^{D_1 \times D_2}$, there exists pseudo-inverse $\mathbf{A}^{\dagger} \in \mathbb{R}^{D_2 \times D_1}$ that satisfies $\mathbf{A}\mathbf{A}^{\dagger}\mathbf{A} = \mathbf{A}$. Considering degraded image: $\mathbf{y} = \mathbf{A}\mathbf{x}$. For any prediction $\hat{\mathbf{x}}_r$, we let $\hat{\mathbf{x}} = \mathbf{A}^{\dagger}\mathbf{y} + (\mathbf{I} - \mathbf{A}^{\dagger}\mathbf{A})\hat{\mathbf{x}}_r$, then immediately gives: $\mathbf{A}\hat{\mathbf{x}} = \mathbf{A}\mathbf{A}^{\dagger}\mathbf{y} + \mathbf{0} = \mathbf{A}\mathbf{x}$, which we make predicted images have the same degradation as original images. This can be regarded as \mathbf{x}_r predicting the zero-space while remaining the original rang-space $\mathbf{A}\mathbf{x}$. For getting the $\hat{\mathbf{x}}_r$, we can employ $\mathbf{A}^{\dagger}\mathbf{y}$ which is the range-space part of \mathbf{x} as biased ground truth and build a joint distribution

$$p_{\beta,\theta}(\mathbf{A}^{\dagger}\mathbf{y}, \mathbf{z}) = p_{\theta}(\mathbf{z})p(\mathbf{A}^{\dagger}\mathbf{y}|\mathbf{A}^{\dagger}\mathbf{A}g_{\beta}(\mathbf{z})). \quad (5)$$

However the $p_{\theta}(\mathbf{z})$ may not be powerful enough to handle image restoration. Recall that we have an EBM in data space, hence we can construct a more powerful prior via neural transport, i.e.,

$$p_{\theta,\omega}(\mathbf{z}) \propto \exp(-E_{\omega}(g_{\beta}(\mathbf{z})))p_{\theta}(\mathbf{z}) \propto \exp(-E_{\beta,\omega}(\mathbf{z}))p_{\theta}(\mathbf{z}). \quad (6)$$

This is achieved by transporting \mathbf{z} to data space via decoder, then the EBM defined in data space is used, finally, the EBM defined in latent space for enhancing prior is well-constructed. By substituting the prior in Eq. (6) into Eq. (5), the new joint likelihood is obtained. Then we run MCMC on \mathbf{z} to maximize the biased joint likelihood, i.e.,

$$g_{\beta}(\mathbf{z}_r^{k+1}) = g_{\beta}(\mathbf{z}_r^k) + \frac{\delta}{2} \nabla_{\mathbf{z}_r^k} \log p_{\theta,\beta,\omega}(\mathbf{A}^{\dagger}\mathbf{y}, \mathbf{z}_r^k) + \sqrt{\delta}\xi, \quad (7)$$

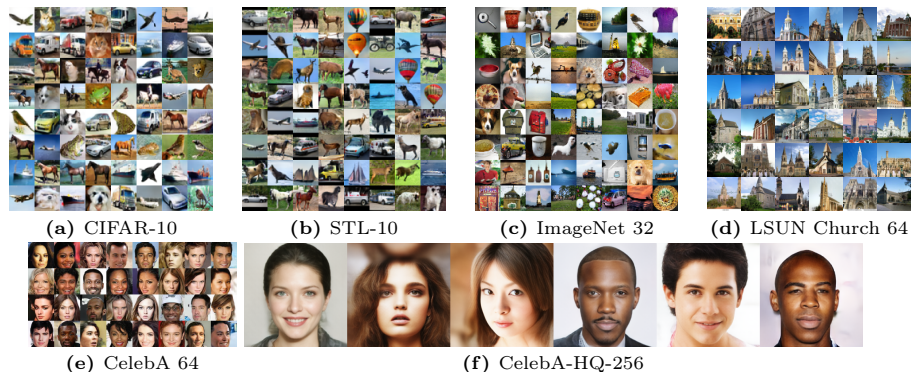


Fig. 1: Random generated samples from EC-VAE. For CelebA 64 and CelebA-HQ-256, we pick out samples for diversity.

where $\xi \sim \mathcal{N}(0, \mathbf{I})$, \mathbf{z}_r^0 can be initialized by sampling from $p_\theta(\mathbf{z})$. In practice, the linear degraded operator \mathbf{A} has various corresponding image restoration tasks, such as colorization, super-resolution, and inpainting. See Appendix B for concrete forms of \mathbf{A} and \mathbf{A}^\dagger . It’s worth noting that our proposed method doesn’t need extra training for those tasks.

5 Experiment

In this section, we conduct comprehensive experiments to evaluate the proposed EC-VAE. We also evaluate the extension of Energy-based calibration to normalizing flow and variational inference. We use a simple ResNet [17] similar to used in VAEBM [53] or CLEL [32] as energy functions E_ω with 30 MCMC steps on CIFAR-10 and 15 MCMC steps on other datasets in all experiments. We adopt Fréchet Inception Distance (FID) [18] as quantitative metrics in most experiments. We apply Exponential Moving Average (EMA) with coefficient of 0.999 on Church-64 and 0.9999 on other datasets for VAE. Please note that by default, our proposed model does not incorporate the use of MCMC in test time, unless specifically indicated otherwise. The prior $p_\theta(\mathbf{z})$ is a simple Gaussian as default.

5.1 Image Generation

In this section, we evaluate EC-VAE on six datasets, including CIFAR-10 [60], STL-10 [5], ImageNet 32 [4,7], LSUN Church 64 [60], CelebA 64 [36], and CelebA-HQ-256 [36]. The backbone similar to that proposed in FastGAN [35] is used in experiments. We use a flow as the prior in experiments on the CelebA-HQ-256. See Appendix C for more experiment setting details. We show qualitative results in Fig. 1. See Appendix F for more qualitative results and qualitative comparison to other models. The quantitative results are reported in Tabs. 1 to 6, with the best results for GANs or Score-models highlighted by underlining, and the best results for other models in bold, respectively.

Our results are comparable to advanced GANs and Score-based Models, outperforming NVAE-family (including NVAE, NCP-VAE and VAEBM) and Glow,

Table 1: Generative performance on CIFAR-10. The † means without extra hyper-parameters tuning. The * means we evaluate the FID by officially released pre-trained checkpoint.

	Model	NFE↓	FID↓	Times (s)↓
Score-based	NCSN [46]	1000	25.32	107.9
	Denosing Diffusion [20]	1000	3.17	80.5
	Consistency Models (LPIPS) [45]	1	8.70	-
GAN-based	SN-GAN [38]	1	21.7	-
	AutoGAN [13]	1	12.4	-
	StyleGAN2 w/o ADA [25]	1	9.9	0.04
VAEs+GANs	VAE+GAN [43]	1	39.8	-
	DC-VAE [43]	1	17.9	-
EBMs+GANs	FlowCE [11]	1	37.3	-
	Divergence Triangle [15]	1	30.1	-
Flow-based	Glow [27]	1	48.9	-
	SurVAE Flow [39]	1	49.03	-
NVAE-family	NVAE [50]	1	50.97	0.36
	NCP-VAE [1]	-	24.08	-
Energy-based	IGEBM [10]	60	40.58	-
	CoopFlow [58]	31	15.80 (26.54†*)	-
	CoopFlow w/o MCMC	1	79.45*	-
	Hat EBM [19]	51	19.30	-
	NT-EBM w/ Flow [40]	-	78.12	-
	CLEL-Large [32]	1200	8.61	-
	Dual MCMC [6]	31	9.26	-
	Diffusion EBM [11]	180	9.58	-
VAEBM [53]	16	12.19	8.79	
Ours	EC-VAE	1	5.20	0.03
	EC-Flow	1	31.12	0.37
Ablations	EC-VAE w/ MCMC	31	5.63	0.52
	EC-Flow w/ MCMC	31	22.74	0.86
	VAE	1	104.68	0.03
	Flow	1	91.33	0.37

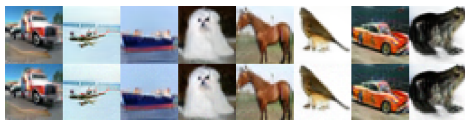


Fig. 2: Comparison of **EC-VAE** (Top) and **EC-VAE (w/ MCMC)** (Bottom) on CIFAR-10. Best viewed when zoomed in.

the most advanced Hierarchical VAE and flows, respectively, by a significant margin on all datasets, despite using much smaller latent space, and much fewer training resources. Our results also outperform existing EBMs, with a *single-step generation manner*. Additionally, Our results outperform the Consistency Models with Learned Perceptual Image Patch Similarity (LPIPS) [61] which is a strong model on single-step non-adversarial generation. Note our approach does not rely on LPIPS, which is known to potentially manipulate the FID metric [31]. Remarkably, we obtain a strong result of unconditional generation on ImageNet 32, even outperforming DDPM [23]. This indicates the strong potential and capability of our proposed model for learning highly diverse datasets.

Comparison with Other EBMs. The proposed method presents a crucial, clear difference from existing methods: we demonstrate that it is possible to drop MCMC steps during test time sampling without compromising the quality

Table 2: Generative performance on STL-10.

Model	FID↓
ProbGAN [16]	46.7
SN-GAN [38]	40.1
Improv. MMD GAN [51]	37.6
AutoGAN [13]	<u>31.0</u>
DC-VAE [43]	41.91
EC-VAE (Ours)	8.39

Table 3: Generative performance on ImageNet 32.

Model	FID↓
DDPM [23]	6.99
Flow Matching [34]	<u>5.02</u>
PixelCNN [41]	40.51
CF-EBM [62]	26.31
CLEL-Large [32]	15.47
EC-VAE (Ours)	5.76

Table 4: Generative performance on Church 64.

Model	FID↓
NVAE [50]	41.3
GLOW [27]	59.35
Diffusion EBM [12]	7.02
Dual MCMC [6]	4.56
VAEBM [53]	13.51
EC-VAE (ours)	4.28

Table 5: Generative performance on CelebA 64.

Model	FID↓
NCSNv2 [47]	26.86
COCO-GAN [33]	<u>4.0</u>
QA-GAN [42]	6.42
Divergence Triangle [15]	24.7
Dual MCMC [6]	5.15
VAEBM [53]	5.31
NCP-VAE [1]	5.25
NVAE [50]	14.74
EC-VAE (Ours)	2.71

Table 6: Generative performance on CelebA-HQ-256.

Model	FID↓
ALAE [44]	19.21
DC-VAE [43]	15.81
PGGAN [24]	<u>8.03</u>
GLOW [27]	68.93
Dual MCMC [6]	15.89
VAEBM [53]	20.38
NCP-VAE [1]	24.79
NVAE [50]	45.11
EC-VAE (Ours)	12.35

of generation. And the FID is even better without MCMC. This is likely because MCMC introduces noise at each step which cannot be perfectly denoised (See Fig. 2), resulting in noise still present in the image. In contrast, the decoder minimizes the distance $\mathbb{E}_{\mathbf{x}} \|\tilde{\mathbf{x}}, \mathbf{x}\|_2^2$, assuming $\tilde{\mathbf{x}} = \mathbf{y} + \xi$, where ξ is zero-mean random noise without any information. The minimum is ideally achieved at $\mathbf{x} = \mathbf{y}$, allowing the decoder to act as a filter and output sharp images without noise. Moreover, as observed, most previous EBMs [10, 53, 58] need to tune MCMC steps and step size carefully during inference to achieve high performance (e.g., CoopFlow[†] in Tab. 1), while our method does not need extra hyper-parameters tuning as even no MCMC required during inference.

Energy-Calibrated Normalizing Flow. We evaluate the EC-Flow on CIFAR-10. We use Glow as the flow architecture. As shown in Tab. 1, the EC-Flow outperforms existing flows in single-step generation, even outperforming the FlowCE which is trained by playing an adversarial game. However, we found that in the case of EC-Flow, the role of MCMC remains crucial in enhancing generative performance. Specifically, EC-Flow w/ MCMC significantly improves the FID from 31.12 to 22.74. We believe that this is due to the expressivity limitations of invertible transformations in flows. Nevertheless, compared to CoopFlow which also combines flows and EBMs, our EC-Flow beat CoopFlow without MCMC by a large margin, demonstrating the effectiveness of the proposed EC-Flow. Note that the 15.8 FID achieved by CoopFlow needs extra hyper-parameter tuning, its result (26.54 FID) without extra tuning is worse than ours w/ MCMC (22.74 FID).



Fig. 3: Qualitative results of zero-shot image restoration (colorization, inpainting, $4\times$ super-resolution).

Table 7: Quantitative results Calibrated posterior on CIFAR-10.

Model	FID↓	MSE↓	ELBO↑
VAE	104.68	0.0235	-953.43
+ Calibrated posterior	102.10	0.0198	-349.14
EC-VAE	5.20	0.0193	652.59
+ Calibrated posterior	5.81	0.0170	1072.40

Table 8: Sampling efficiency and training cost on CIFAR-10. Time is the seconds took to generate 50 images.

Model	FID↓	Latent dim↓	Time↓	GPU days ↓	GPU-Type
NCSN	25.32	3072	107.9	-	-
GLOW [39]	48.9	3072	-	60	-
SurVAE Flow [39]	49.03	1536	-	7	TITAN-X
NVAE [50]	50.97	153600	0.36	18.3	32G-V100
NCP-VAE [1]	24.08	153600	-	34.5	32G-V100
VAEBM [53]	12.19	153600	8.79	>18.3	32G-V100
EC-VAE w/ MCMC (ours)	5.63	128	0.52	3	RTX-3090
EC-VAE (ours)	5.20	128	0.03	3	RTX-3090

Energy-Calibrated Variational Learning. We also evaluate Energy-Calibrated Variational Learning on CIFAR-10, with 5 MCMC steps for calibrating posterior. As shown in Tab. 7, the calibrated posterior consistently enhances the ELBO and MSE of related baseline VAE and EC-VAE. This indicates that the calibrated posterior can provide a more accurate posterior for better likelihood maximization. However, a slight FID deterioration is observed in the EC-VAE with Calibrated posterior, implying that the likelihood is not always consistent with generation quality. Interestingly, we found the EC-VAE also improves the ELBO and MSE compared to VAE, despite we only calibrate the generative side. This may be highly due to the energy-based calibration effectively improving the ability to map latent space to data space and reducing the gap between prior and aggregated posterior.

5.2 Sampling Efficiency and Training Cost

Although the score-based model and NVAE’s variants have shown outstanding sample quality, their sampling speed is limited by the necessity of expensive MCMC sampling steps. As shown in Tab. 8, the generation by EC-VAE, in contrast, takes just one pass, making it hundreds of and thousands of times faster than NCSN and VAEBM, respectively. Notably, even after performing MCMC steps, our method still only requires 0.52 seconds to generate 50 samples. This is because our energy network is lightweight and only requires 30 MCMC steps on the data space, while VAEBM runs MCMC in (\mathbf{x}, \mathbf{z}) space which requires backward through its heavy decoder at each step. Furthermore, due to the extremely large scale of latent variables used in NVAE-family and previous flows, yielding challenges in learning, they need at least 7 GPU days to be trained on

Table 9: Quantitative results of image restoration on CelebA-HQ.

Model	4× SR		Colorization	
	PSNR↑	FID↓	Cons↓	FID↓
PULSE [37]	22.7	40.3	N/A	
DDRM [26]	31.6	31.0	456	31.2
DDNM [52]	31.6	22.3	26.2	26.4
EC-VAE (ours)	28.8	30.4	0.004	13.3

Table 10: Comparison for FID on CIFAR-10 between several related methods.

Model	FID↓
EC-VAE	5.20
EC-VAE w/ flow prior	4.85
EC-VAE w/ LPIPS	4.77
EC-VAE w/o primal-dual	5.72
VAE	104.68
EBM	45.52
EBM init w/ VAE samples	44.63
VAE + WGAN	33.78

CIFAR-10, while our model only needs 3 GPU days despite using costly MCMC steps in training.

5.3 Image Restoration

Here we show that well-trained EC-VAE is able to be zero-shot used in image restoration as described in Sec. 4.3. The Qualitative results are shown in Fig. 3. Our model can successfully restore those images with high quality and consistency. More qualitative results can be found in Appendix F. Following the setting as in [52], we compare our method with strong zero-shot baselines, using metrics FID, PSNR, and Consistency [52] (i.e., $\|\mathbf{A}\hat{\mathbf{x}} - \mathbf{A}\mathbf{x}\|_1$). As shown in Tab. 9, we outperform GAN-based PULSE [37] and compete with diffusion-based DDNM [52] and DDRM [26], which confirms our model provides competitive performance.

5.4 Ablation Study

All experiments here are performed on CIFAR-10 for faster training. See Appendix E for Experimental settings and additional ablations.

Effect of Calibration. The proposed method is calibrating generative models by incorporating generated samples into training. This raises the question of what is the performance of single generative model and train generative model and EBMs as independent components. We compare the proposed EC-VAE with three related baselines i.e., VAE, EBM, and EBM initialized with pre-trained VAE samples. As shown in Table. 10, we significantly outperform these three variants by a huge margin. Note that there is almost no benefit of initializing EBM with pre-trained VAE samples, implying the effectiveness of calibration.

Energy-based calibration vs. Adversarial-based Calibration. The gradient for updating EBMs E_ω is similar to the gradient updates of WGAN’s discriminator [2]. The key difference is that the EBMs draw samples from E_ω by MCMC, while WGAN draws negative samples from a generator. WGAN updates the generator and discriminator by adversarial training, while we update EBMs by maximizing the likelihood and we update the VAE by maximizing adaptive weight between the lower bound of data likelihood and conditional likelihood on calibrated samples (i.e., $\log p(\tilde{\mathbf{x}}|\mathbf{x}) = -\frac{\|\tilde{\mathbf{x}} - \mathbf{x}\|_2^2}{2\sigma^2} + \text{Constant}$). Thus, a related variant of EC-VAE is updating the VAE by both ELBO and WGAN training objectives. We compare the adversarial variant with the proposed EC-VAE. As

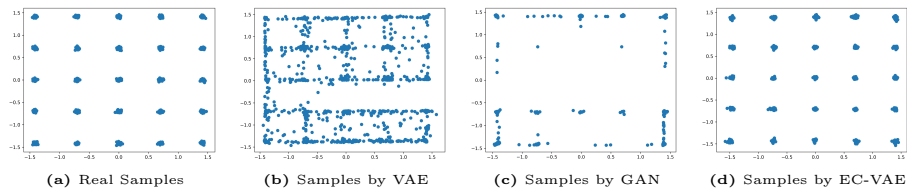


Fig. 4: Qualitative results on the 25-Gaussians dataset.

shown in Table. 10, the adversarial variant achieves similar results (**33.78 FID**) to the VAEs+GANs (**39.8 FID**) in DC-VAE which is significantly worse than the proposed EC-VAE (**5.20 FID**), highlighting the advantage of our method compared to adversarial training.

Effect of Primal-Dual. We firstly emphasize that primal-dual has advantages with theoretical guarantees in constrained learning [3]. This section is for empirically showing the impact intuitively. As shown in Tab. 10, in comparison to primal-dual, the naive stochastic gradient descent (w/o dual variable λ) algorithm yields worse results.

Compatibility with Advanced Technique in VAEs. We employ MSE as the distance metric and a Gaussian as prior in CIFAR-10. Recognizing the efficacy of flexible priors and better distance metrics in improving vanilla VAEs [1, 54], we investigate the impact of integrating either flow prior or LPIPS into the EC-VAE. The superior performance of both variants (Tab. 10) suggests that EC-VAE is orthogonal to these advanced techniques to some extent. Additionally, we note that the improvement margin is not large, indicating that EC-VAE effectively addressed the prior hole issue and blurry generation issue in vanilla VAEs.

5.5 Extra Study on Mode Coverage

We evaluate the mode coverage of our model on the popular 25-Gaussians. This 2D toy dataset is also used in previous work [53]. We train our EC-VAE with 15 MCMC steps and compare it to other models in Fig. 4. The VAE’s encoder, decoder, and energy function both consist of four linear layers with 256 hidden units. The latent dimension is 20. We observe that the vanilla VAEs can not produce good samples, lots of samples are significantly out of modes. In contrast, our EC-VAE successfully calibrated the sampling distribution with all modes covered and high-quality samples. We also train a GAN with similar networks for comparison. We observe that GAN suffers severely from mode collapse. Moreover, as the true distribution is available, we also evaluate the likelihood of 100000 generated samples by models with true data density. Our EC-VAE obtains **-1.07 nats** which significantly improves the likelihood obtained by VAE which is **-1.78 nats**. For reference, the likelihood of 100000 real data under real density is **-1.04 nats**.

6 Conclusion

In this paper, we proposed EC-VAE, using conditional EBMs for calibrating the VAEs. Furthermore, the proposed energy-based calibration can enhance normal-

izing flows and variational posterior. We also propose and show that EC-VAE can effectively solve image restoration in a zero-shot manner. We show that MCMC sampling is not required once the VAE is calibrated while keeping high performance. In terms of efficiency, EC-VAE can be trained by a single GPU and is fast to converge, addressing the intensive computational resources consumption problem of previous state-of-the-art VAEs (i.e., NVAE). The proposed EC-VAE shows promising results over multiple datasets with high computational efficiency, significantly reducing the gap with GANs.

References

1. Aneja, J., Schwing, A., Kautz, J., Vahdat, A.: A contrastive learning approach for training variational autoencoder priors. *Advances in Neural Information Processing Systems* **34** (2021) [2](#), [10](#), [11](#), [12](#), [14](#)
2. Arjovsky, M., Chintala, S., Bottou, L.: Wasserstein generative adversarial networks. In: Precup, D., Teh, Y.W. (eds.) *Proceedings of the 34th International Conference on Machine Learning*. *Proceedings of Machine Learning Research*, vol. 70, pp. 214–223. PMLR (06–11 Aug 2017), <https://proceedings.mlr.press/v70/arjovsky17a.html> [13](#)
3. Chamon, L.F., Paternain, S., Calvo-Fullana, M., Ribeiro, A.: Constrained learning with non-convex losses. *arXiv:2103.05134* (2021) [7](#), [14](#)
4. Chrabaszcz, P., Loshchilov, I., Hutter, F.: A downsampled variant of imagenet as an alternative to the cifar datasets. *ArXiv* **abs/1707.08819** (2017), <https://api.semanticscholar.org/CorpusID:7304542> [9](#)
5. Coates, A., Ng, A., Lee, H.: An analysis of single-layer networks in unsupervised feature learning. In: *AISTATS*. pp. 215–223 (2011) [9](#)
6. Cui, J., Han, T.: Learning energy-based model via dual-mcmc teaching. *Advances in Neural Information Processing Systems* **36** (2024) [4](#), [10](#), [11](#), [3](#)
7. Deng, J., Dong, W., Socher, R., Li, L.J., Li, K., Fei-Fei, L.: Imagenet: A large-scale hierarchical image database. In: 2009 IEEE Conference on Computer Vision and Pattern Recognition (Jun 2009). <https://doi.org/10.1109/cvpr.2009.5206848>, <http://dx.doi.org/10.1109/cvpr.2009.5206848> [9](#)
8. Dinh, L., Krueger, D., Bengio, Y.: NICE: non-linear independent components estimation. In: Bengio, Y., LeCun, Y. (eds.) *3rd International Conference on Learning Representations, ICLR 2015, San Diego, CA, USA, May 7-9, 2015, Workshop Track Proceedings* (2015), <http://arxiv.org/abs/1410.8516> [1](#)
9. Dinh, L., Sohl-Dickstein, J., Bengio, S.: Density estimation using real nvp. *arXiv preprint arXiv:1605.08803* (2016) [1](#)
10. Du, Y., Mordatch, I.: Implicit generation and modeling with energy based models. In: *Advances in Neural Information Processing Systems*. pp. 3608–3618 (2019) [1](#), [10](#), [11](#), [2](#)
11. Gao, R., Nijkamp, E., Kingma, D.P., Xu, Z., Dai, A.M., Wu, Y.N.: Flow contrastive estimation of energy-based models. In: *Proceedings of the IEEE/CVF Conference on Computer Vision and Pattern Recognition*. pp. 7518–7528 (2020) [10](#)
12. Gao, R., Song, Y., Poole, B., Wu, Y.N., Kingma, D.P.: Learning energy-based models by diffusion recovery likelihood. *arXiv preprint arXiv:2012.08125* (2020) [4](#), [11](#)
13. Gong, X., Chang, S., Jiang, Y., Wang, Z.: Autogan: Neural architecture search for generative adversarial networks. In: *ICCV* (2019) [10](#), [11](#)

14. Goodfellow, I., Pouget-Abadie, J., Mirza, M., Xu, B., Warde-Farley, D., Ozair, S., Courville, A., Bengio, Y.: Generative adversarial nets. *Advances in neural information processing systems* **27** (2014) [1](#)
15. Han, T., Nijkamp, E., Zhou, L., Pang, B., Zhu, S.C., Wu, Y.N.: Joint training of variational auto-encoder and latent energy-based model. In: *Proceedings of the IEEE/CVF Conference on Computer Vision and Pattern Recognition*. pp. 7978–7987 (2020) [4](#), [10](#), [11](#)
16. He, H., Wang, H., Lee, G.H., Tian, Y.: Probgan: Towards probabilistic gan with theoretical guarantees. In: *ICLR* (2019) [11](#)
17. He, K., Zhang, X., Ren, S., Sun, J.: Deep residual learning for image recognition. In: *Proceedings of the IEEE Conference on Computer Vision and Pattern Recognition (CVPR)* (June 2016) [9](#)
18. Heusel, M., Ramsauer, H., Unterthiner, T., Nessler, B., Hochreiter, S.: Gans trained by a two time-scale update rule converge to a local nash equilibrium. In: *Advances in neural information processing systems*. pp. 6626–6637 (2017) [9](#)
19. Hill, M., Nijkamp, E., Mitchell, J.C., Pang, B., Zhu, S.C.: Learning probabilistic models from generator latent spaces with hat EBM. In: Oh, A.H., Agarwal, A., Belgrave, D., Cho, K. (eds.) *Advances in Neural Information Processing Systems* (2022), https://openreview.net/forum?id=AluQNIb_Zy [4](#), [10](#)
20. Ho, J., Jain, A., Abbeel, P.: Denoising diffusion probabilistic models. *arXiv preprint arXiv:2006.11239* (2020) [10](#)
21. Huang, H., He, R., Sun, Z., Tan, T., et al.: Introvae: Introspective variational autoencoders for photographic image synthesis. *Advances in neural information processing systems* **31** (2018) [2](#)
22. Ioffe, S., Szegedy, C.: Batch normalization: Accelerating deep network training by reducing internal covariate shift. *CoRR* **abs/1502.03167** (2015), <http://arxiv.org/abs/1502.03167> [2](#)
23. Jonathan, H., Jain, A., Abbeel, P.: Denoising diffusion probabilistic models. *Advances in Neural Information Processing Systems* **33**, 6840–6851 (2020) [1](#), [10](#), [11](#)
24. Karras, T., Aila, T., Laine, S., Lehtinen, J.: Progressive growing of GANs for improved quality, stability, and variation. In: *International Conference on Learning Representations* (2018) [11](#)
25. Karras, T., Aittala, M., Hellsten, J., Laine, S., Lehtinen, J., Aila, T.: Training generative adversarial networks with limited data. *arXiv preprint arXiv:2006.06676* (2020) [10](#), [3](#)
26. Kawar, B., Elad, M., Ermon, S., Song, J.: Denoising diffusion restoration models. In: *Advances in Neural Information Processing Systems* (2022) [13](#)
27. Kingma, D.P., Dhariwal, P.: Glow: Generative flow with invertible 1x1 convolutions. *arXiv preprint arXiv:1807.03039* (2018) [10](#), [11](#)
28. Kingma, D.P., Welling, M.: Auto-encoding variational bayes. In: *The International Conference on Learning Representations (ICLR)* (2014) [1](#)
29. Kingma, D.P., Welling, M.: Stochastic gradient vb and the variational auto-encoder. In: *Second International Conference on Learning Representations, ICLR*. vol. 19, p. 121 (2014) [3](#)
30. Kong, Z., Chaudhuri, K.: The expressive power of a class of normalizing flow models. *International Conference on Artificial Intelligence and Statistics, International Conference on Artificial Intelligence and Statistics* (May 2020) [1](#)
31. Kynkäänniemi, T., Karras, T., Aittala, M., Aila, T., Lehtinen, J.: The role of imagenet classes in fréchet inception distance. In: *The Eleventh International Con-*

- ference on Learning Representations (2023), https://openreview.net/forum?id=4oXTQ6m_ws8 10
32. Lee, H., Jeong, J., Park, S., Shin, J.: Guiding energy-based models via contrastive latent variables. In: The Eleventh International Conference on Learning Representations (2023), <https://openreview.net/forum?id=CZmHHj9MgkP> 2, 9, 10, 11
 33. Lin, C.H., Chang, C.C., Chen, Y.S., Juan, D.C., Wei, W., Chen, H.T.: Coco-gan: generation by parts via conditional coordinating. In: Proceedings of the IEEE International Conference on Computer Vision. pp. 4512–4521 (2019) 11
 34. Lipman, Y., Chen, R.T.Q., Ben-Hamu, H., Nickel, M., Le, M.: Flow matching for generative modeling. In: The Eleventh International Conference on Learning Representations (2023), <https://openreview.net/forum?id=PqvMRDCJT9t> 11
 35. Liu, B., Zhu, Y., Song, K., Elgammal, A.: Towards faster and stabilized gan training for high-fidelity few-shot image synthesis. In: International Conference on Learning Representations (2020) 9
 36. Liu, Z., Luo, P., Wang, X., Tang, X.: Deep learning face attributes in the wild. In: Proceedings of the IEEE international conference on computer vision. pp. 3730–3738 (2015) 9
 37. Menon, S., Damian, A., Hu, S., Ravi, N., Rudin, C.: Pulse: Self-supervised photo upsampling via latent space exploration of generative models. In: Proceedings of the IEEE/CVF conference on computer vision and pattern recognition. pp. 2437–2445 (2020) 13
 38. Miyato, T., Kataoka, T., Koyama, M., Yoshida, Y.: Spectral normalization for generative adversarial networks. In: ICLR (2018) 10, 11
 39. Nielsen, D., Jaini, P., Hoogeboom, E., Winther, O., Welling, M.: Survae flows: Surjections to bridge the gap between vaes and flows. In: NeurIPS (2020) 10, 12
 40. Nijkamp, E., Gao, R., Sountsov, P., Vasudevan, S., Pang, B., Zhu, S.C., Wu, Y.N.: MCMC should mix: Learning energy-based model with neural transport latent space MCMC. In: International Conference on Learning Representations (2022), <https://openreview.net/forum?id=4C93Qvn-tz> 10
 41. van den Oord, A., Kalchbrenner, N., Vinyals, O., Espenholt, L., Graves, A., Kavukcuoglu, K.: Conditional image generation with pixelcnn decoders (2016) 11
 42. Parimala, K., Channappayya, S.: Quality aware generative adversarial networks. In: Advances in Neural Information Processing Systems. pp. 2948–2958 (2019) 11
 43. Parmar, G., Li, D., Lee, K., Tu, Z.: Dual contradistinctive generative autoencoder. In: Proceedings of the IEEE/CVF Conference on Computer Vision and Pattern Recognition (CVPR). pp. 823–832 (June 2021) 2, 10, 11
 44. Pidhorskyi, S., Adjeroh, D.A., Doretto, G.: Adversarial latent autoencoders. In: Proceedings of the IEEE/CVF Conference on Computer Vision and Pattern Recognition. pp. 14104–14113 (2020) 11
 45. Song, Y., Dhariwal, P., Chen, M., Sutskever, I.: Consistency models (2023) 10, 3
 46. Song, Y., Ermon, S.: Generative modeling by estimating gradients of the data distribution. In: Advances in Neural Information Processing Systems. pp. 11918–11930 (2019) 10
 47. Song, Y., Ermon, S.: Improved techniques for training score-based generative models. arXiv preprint arXiv:2006.09011 (2020) 11, 3
 48. Tomczak, J.M., Welling, M.: VAE with a vampprior. In: Storkey, A.J., Pérez-Cruz, F. (eds.) International Conference on Artificial Intelligence and Statistics, AISTATS 2018, 9-11 April 2018, Playa Blanca, Lanzarote, Canary Islands, Spain. Proceedings of Machine Learning Research, vol. 84, pp. 1214–1223. PMLR (2018), <http://proceedings.mlr.press/v84/tomczak18a.html> 2

49. Tzeng, E., Hoffman, J., Saenko, K., Darrell, T.: Adversarial discriminative domain adaptation. In: Proceedings of the IEEE conference on computer vision and pattern recognition. pp. 7167–7176 (2017) [2](#)
50. Vahdat, A., Kautz, J.: NVAE: A deep hierarchical variational autoencoder. In: Neural Information Processing Systems (NeurIPS) (2020) [2](#), [4](#), [10](#), [11](#), [12](#)
51. Wang, W., Sun, Y., Halgamuge, S.: Improving mmd-gan training with repulsive loss function. In: ICLR (2019) [11](#)
52. Wang, Y., Yu, J., Zhang, J.: Zero-shot image restoration using denoising diffusion null-space model. In: International Conference on Learning Representations (2023), <https://openreview.net/forum?id=mRieQgMtNTQ> [8](#), [13](#)
53. Xiao, Z., Kreis, K., Kautz, J., Vahdat, A.: Vaebm: A symbiosis between variational autoencoders and energy-based models. In: International Conference on Learning Representations (2021) [4](#), [9](#), [10](#), [11](#), [12](#), [14](#)
54. Xiao, Z., Yan, Q., Chen, Y., Amit, Y.: Generative latent flow: A framework for non-adversarial image generation. CoRR [abs/1905.10485](https://arxiv.org/abs/1905.10485) (2019), [http://arxiv.org/abs/1905.10485](https://arxiv.org/abs/1905.10485) [14](#)
55. Xie, J., Lu, Y., Gao, R., Wu, Y.N.: Cooperative learning of energy-based model and latent variable model via mcmc teaching. In: Proceedings of the AAAI Conference on Artificial Intelligence. vol. 32 (2018) [4](#), [3](#)
56. Xie, J., Lu, Y., Zhu, S.C., Wu, Y.: A theory of generative convnet. In: International Conference on Machine Learning. pp. 2635–2644 (2016) [1](#)
57. Xie, J., Zheng, Z., Li, P.: Learning energy-based model with variational auto-encoder as amortized sampler. In: Proceedings of the AAAI Conference on Artificial Intelligence. vol. 35, pp. 10441–10451 (2021) [4](#), [2](#), [3](#)
58. Xie, J., Zhu, Y., Li, J., Li, P.: A tale of two flows: Cooperative learning of langevin flow and normalizing flow toward energy-based model. In: International Conference on Learning Representations (2022), <https://openreview.net/forum?id=31d5RLCUuXC> [4](#), [10](#), [11](#), [2](#)
59. Yang, G., Huang, X., Hao, Z., Liu, M.Y., Belongie, S., Hariharan, B.: Pointflow: 3d point cloud generation with continuous normalizing flows. In: Proceedings of the IEEE/CVF international conference on computer vision. pp. 4541–4550 (2019) [2](#)
60. Yu, F., Seff, A., Zhang, Y., Song, S., Funkhouser, T., Xiao, J.: Lsun: Construction of a large-scale image dataset using deep learning with humans in the loop. arXiv preprint [arXiv:1506.03365](https://arxiv.org/abs/1506.03365) (2015) [9](#)
61. Zhang, R., Isola, P., Efros, A.A., Shechtman, E., Wang, O.: The unreasonable effectiveness of deep features as a perceptual metric. In: CVPR (2018) [10](#)
62. Zhao, Y., Xie, J., Li, P.: Learning energy-based generative models via coarse-to-fine expanding and sampling. In: International Conference on Learning Representations (2021), https://openreview.net/forum?id=aD1_5zowqV [11](#)

A Pseudo Code of Proposed Algorithm

Algorithm 1: Energy-Calibrated VAE Algorithm.

input : Learning iterations T , number of MCMC steps K , observed examples $\{\mathbf{x}_i\}_{i=1}^N$, network optimizer \mathcal{Q} .
output: Estimated parameters $\phi = \{\alpha, \beta, \theta\}, \omega$.
for $t = 0 : T - 1$ **do**

Primal-Step:

1. **Mini-batch:** Sample observed examples $\{\mathbf{x}_i\}_{i=1}^n$
2. **Mini-batch:** Sample generated examples $\{\hat{\mathbf{x}}_i\}_{i=1}^n$, where $\hat{\mathbf{x}}_i \sim p_{\beta, \theta}(\hat{\mathbf{x}})$
3. **Sample $\tilde{\mathbf{x}}$ by MCMC:** For each generated $\hat{\mathbf{x}}_i$, sample $\tilde{\mathbf{x}}_i$ using Eq. (3) for K steps
4. **Learning** E_ω : $\omega_{t+1} = \mathcal{Q}(\nabla_{\omega_t} \hat{\mathcal{L}}(\omega_t), \omega_t)$
5. **Learning and Calibrating VAE** ϕ_t :
 $\phi_{t+1} = \mathcal{Q}(\nabla_{\phi_t} \hat{\mathcal{L}}(\phi_t) + \lambda \nabla_{\phi_t} \hat{\mathcal{L}}_{\text{con}}(\phi_t), \phi_t)$

Dual-Step:

6. **Update** λ : update λ according to Eq. (4)

B More Details in Zero-Shot Image Restoration

Typical image restoration tasks usually have simple \mathbf{A} and \mathbf{A}^\dagger , we give some examples following:

Colorization. $\mathbf{A} = [1/3, 1/3, 1/3]$ converts each RGB channel pixel $[r, g, b]^T$ into a grayscale value $[r/3 + g/3 + b/3]$. A simple pseudo-inverse \mathbf{A}^\dagger is $\mathbf{A}^\dagger = [1, 1, 1]^T$, that satisfies $\mathbf{A}\mathbf{A}^\dagger\mathbf{A} = \mathbf{A}$.

Super Resolution. For SR with scale n , we can set $\mathbf{A} \in \mathbb{R}^{1 \times n^2}$ as a average-pooling operator $[1/n^2, \dots, 1/n^2]$. A simple pseudo-inverse $\mathbf{A}^\dagger \in \mathbb{R}^{n^2 \times 1}$ is $\mathbf{A}^\dagger = [1, \dots, 1]^T$.

Inpainting. For \mathbf{A} is a mask operator, simply let $\mathbf{A}^\dagger = \mathbf{A}$, we can have $\mathbf{A}\mathbf{A}^\dagger\mathbf{A} = \mathbf{A}$.

C Experiment Setting Details in Image Generation

Evaluation Metric. We employ the FID score as the metric in most experiments. We compute the FID score between 50k generated samples and training images. On CelebA HQ we compute 30k generated samples and training images due to the dataset only containing 30k images.

Dataset Details. For STL-10, we follow the procedure in AutoGAN and DC-VAE, and resize the STL-10 images to 32×32 .

Ablations in Tab. 1. The VAE and Flow use the same architecture as EC-VAE and EC-Flow, except the EBM is not needed in VAE and Flow.

Energy-Calibrated Variational Learning. We use five MCMC steps for calibrating the posterior. We employ exactly the same architecture of VAE and EBM

(only need for EC-VAE and EC-VAE w/ calibrated posterior) for all variants. Both the MSE and ELBO are measured on the test set of CIFAR-10.

Hyper-parameters. Given a large number of datasets, heavy compute requirements, and limited computational resources, we don’t optimize the hyper-parameters carefully. Even if the backbone is not carefully selected or designed, it’s expected that we can use other well-designed backbones to easily get better results. Also, we just roughly choose the learning rate from $1e-4$ or $2e-4$ in all experiments. Following most previous work [10, 32, 58], we utilize the Langevin Dynamics with a low temperature (e.g., $1e-5$) and select a small step size from $1e-6$ or $1e-5$. On all datasets, we train EC-VAE using the Adam optimizer. For a fair comparison, EMA is applied for the VAE component for all variants in our ablations. For all other training details (e.g., detailed model architecture), we refer readers to our full code, which will be released after published.

D Experiment details in Zero-Shot Image Restoration

We use the well-trained **Energy-Calibrated VAE** in zero-shot image restoration by the proposed application method in Sec. 4.3 with 50 MCMC steps.

E Experiment Details in Ablation Study

Setting Details. The same architectural design of VAE’s encoder, decoder, and energy function is consistently applied across all variants of EC-VAE in our ablation studies. For VAE+GAN, the same architectural design of VAE is applied, and we directly use the architecture of energy function as the discriminator. For EBM the same architectural design of energy function is applied. For EBM nit w/ VAE samples, the same architectural design of all networks is applied. For EC-VAE w/ flow prior, we use a glow parameterized by MLPs as the architecture. For EC-VAE w/ LPIPS, we only use LPIPS in modeling $p_\beta(\mathbf{x}|\mathbf{z})$, as we found the benefit of using LPIPS in modeling calibration loss is negligible. We employed a replay buffer size of 10,000 for training the EBM, with a distribution of 5% sampling from noise and 95% sampling from the replay buffer. Regarding the EBM initialized with VAE samples, a similar approach was adopted, utilizing the same replay buffer size of 10,000, 5% sampling from the VAE, and 95% sampling from the replay buffer. Notably, in the absence of a replay buffer during the training of the EBM initialized with VAE samples, we were unable to produce reasonable generation outcomes.

E.1 Additional Ablations

Comparison to CoopVAEBM. We provide an extra comparison with CoopVAEBM [57] which is a cooperative learning approach for training VAE and EBM. As discussed in related work section (Sec. 2.4), the existing cooperative

Table 11: Additional Quantitative results on CIFAR-10.

Model	FID↓	MSE↓	ELBO↑
CoopVAEBM w/ MCMC [57]	22.08	-	-
CoopVAEBM w/o MCMC [57]	26.17	0.0276	130.35
EC-VAE (ours)	5.20	0.0193	652.59

Table 12: Additional Quantitative results on CIFAR-10.

Model	FID↓
EC-VAE	5.20
EC-VAE w/o EMA	8.02
EC-VAE w/ unconditional EBM	5.89

learning approach trains the base generative model (i.e., VAE) solely using generated samples, leading to biased learning. To further emphasize the necessity of training the base generative model (i.e., VAE) upon both real data and generated samples with adaptive weight as proposed in our **EC-VAE**, we train the CoopVAEBM using the same architecture as EC-VAE to ensure a fair comparison instead of directly using the reported results in their original paper which might be influenced by architectural differences. As shown in Tab. 11, our EC-VAE outperforms CoopVAEBM by a large margin in terms of both FID, MSE, and ELBO. Additionally, it is observed that the MCMC still performs an important role in improving the generation quality of CoopVAEBM. These results indicate that our proposed EC-VAE is more effective with more accurate likelihood learning and better generation quality.

Effect of Exponential Moving Average (EMA). The EMA technique has been extensively incorporated into prior generative models [25, 45, 47], which demonstrates its widespread applicability and effectiveness. In alignment with these findings, we found the EMA can also enhance the performance of our model, EC-VAE, as indicated by the improved FID scores. As detailed in Tab. 12, the application of EMA to EC-VAE results in a noteworthy reduction in the FID score from 8.02 to 5.20 on CIFAR-10.

Effect of Conditional Energy-Based Models. Unlike the previous cooperate approach [6, 55, 57] which utilize unconditional EBMs for obtaining MCMC-revised samples, we utilize conditional EBMs to produce calibrated samples. Conditional EBMs have the advantage of constraining the high-density regions to be localized around the condition \mathbf{x} . This not only simplifies the calibrating process for the VAE but also enables us to focus on maximizing the conditional likelihood of the calibrated samples given condition samples via the VAE’s decoder. Otherwise, an additional inference step would be necessary to infer the related latent variables of the MCMC-revised samples, as discussed in CoopVAEBM [57]. Empirical evidence, as presented in Tab. 12, supports the efficacy of conditional EBMs; the FID deteriorates from 5.20 to 5.89 when an unconditional EBM is employed, highlighting the superiority of the conditional approach.

F Additional Qualitative Results

We present additional qualitative results in this section. Note that all images in this section are **un-selected**.

Qualitative Comparison to Other models. We provide a qualitative comparison to other models on CIFAR-10 in Fig. 5. We use the official checkpoint from CoopFlow to generate its samples and use its official code to compute the corresponding FID score. For VAEBM w/o MCMC, we take the samples from its paper’s appendix.

Please see if drop MCMC steps at test time sampling, how better our proposed method is compared to previous cooperative learning model (i.e., CoopFlow) and previous work that combines generative model and EBMs (i.e., VAEBM). And we note that CoopFlow is the most advanced model among existing cooperative learning models. Also, many existing works (e.g., CoopFlow and VAEBM) related to EBMs need extra hyper-parameters tuning stage to achieve high performance or will lead to a significantly worse result. And it can be seen in Fig. 5d that after carefully tuning the hyper-parameters, although the FID is better than the untuned, the color of samples by CoopFlow tends to be over-saturated, which is not the property of real data. In contrast, our proposed Energy-Calibrated VAE can even drop MCMC steps at test time sampling while achieving high-quality samples.

Qualitative Results. From the interpolation results in Fig. 12, we conclude that our model has a good, smooth latent space. We show the nearest neighbors from the training dataset with our generated samples in Fig. 13. It is easy to see our generated images are significantly different from images from the training dataset, which concludes that our model does not simply remember the data.

Additional Zero-Shot Image Restoration samples are in Fig. 6.

Additional samples on CelebA 64 are in Fig. 7.

Additional samples on LSUN Church 64 are in Fig. 8.

Additional samples on STL-10 are in Fig. 9.

Additional samples on ImageNet 32 are in Fig. 10.

Additional samples on CelebA-HQ-256 are in Fig. 11.

Interpolation results on CelebA-HQ-256 are in Fig. 12.

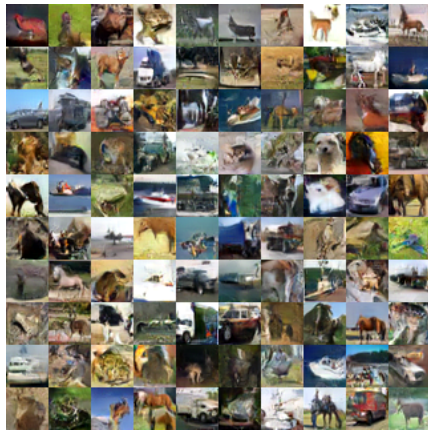
Samples on CelebA-HQ-256 and their nearest neighbors from the training dataset are in Fig. 13.



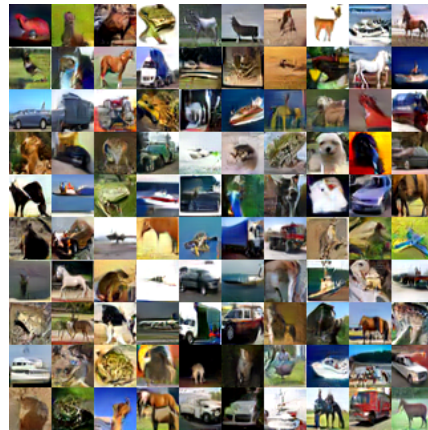
(a) CoopFlow without MCMC (FID=79.45)



(b) VAE BM without MCMC (i.e., NVAE, FID=50.97)



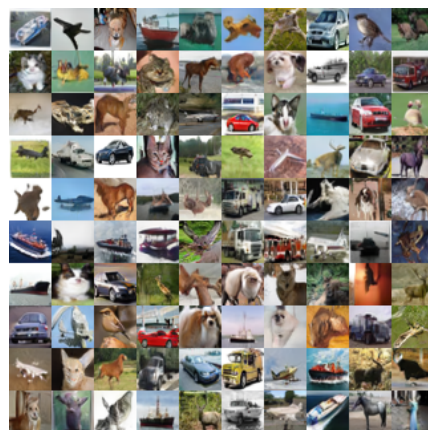
(c) CoopFlow w/o extra tuning hyper-parameters (FID=26.54)



(d) CoopFlow w/ carefully tuned hyper-parameters (FID=15.80)



(e) Real Data



(f) EC-VAE (FID=5.20)

Fig. 5: Qualitative comparison of Energy-Calibrated VAE (Ours) and other models on CIFAR-10. Samples are un-selected.

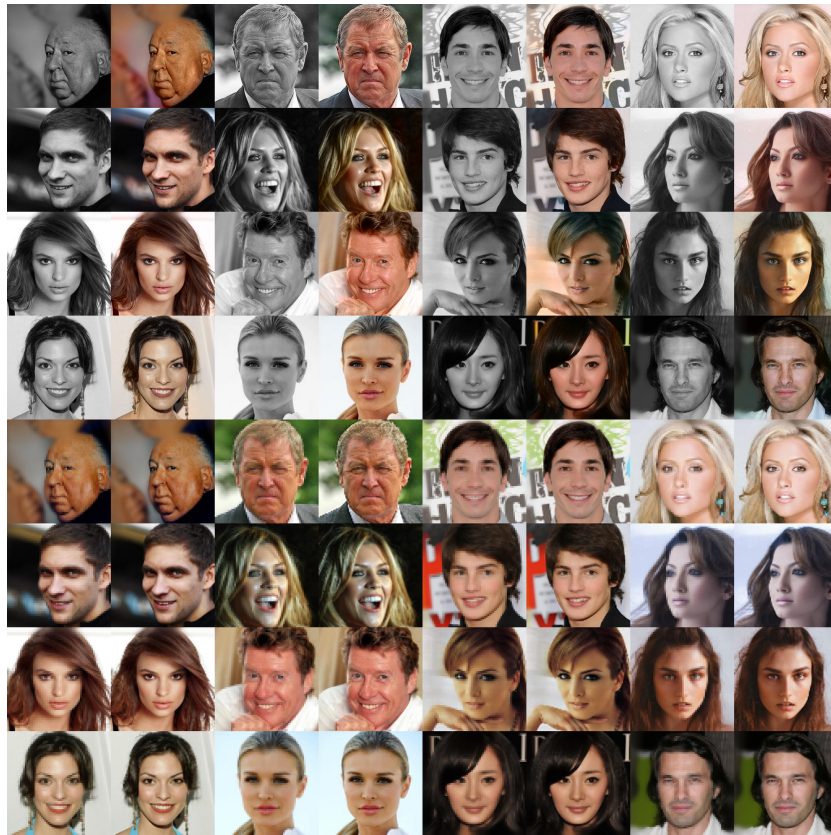


Fig. 6: Additional Zero-Shot Image Restoration (Colorization, $4\times$ SR) Samples on CelebA-HQ-256. Samples are uncurated.



Fig. 7: Additional samples from CelebA 64. Samples are uncurated.



Fig. 8: Additional samples from LSUN Church 64. Samples are uncurated.



Fig. 9: Additional samples from STL-10 which are uncurated.

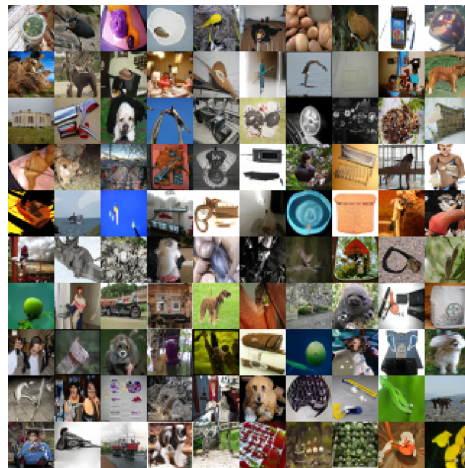


Fig. 10: Additional samples from ImageNet 32 which are uncurated.



Fig. 11: Additional samples from CelebA-HQ-256. Samples are uncurated.

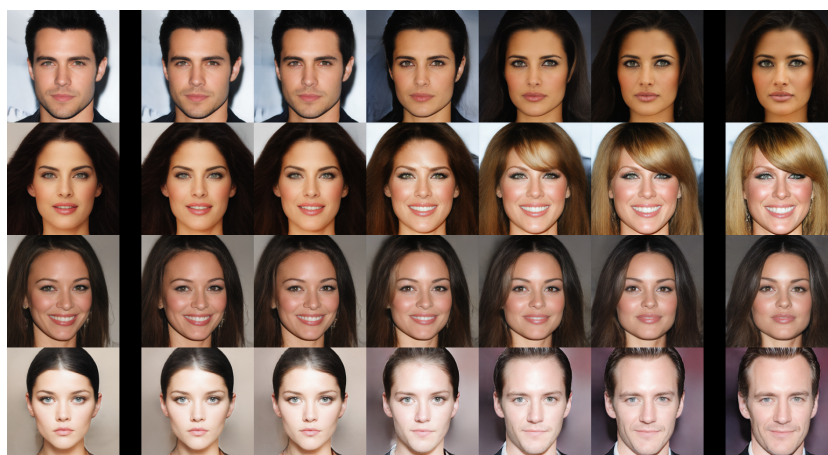


Fig. 12: Interpolation results in latent space on CelebA-HQ-256.



Fig. 13: Generated images (left) and their nearest neighbors in VGG's feature space from the CelebA-HQ-256 training dataset.